Hydrol. Earth Syst. Sci. Discuss., 7, 1033–1072, 2010
www.hydrol-earth-syst-sci-discuss.net/7/1033/2010/

Hydrology and Earth System Sciences Discussions

Simulation of snow accumulation and melt in needleleaf forest environments

C. R. Ellis, J. W. Pomeroy, T. Brown, and J. MacDonald

Centre for Hydrology, University of Saskatchewan, 117 Science Place, Saskatoon, Saskatchewan, S7N 5C8, Canada

Received: 15 January 2010 – Accepted: 22 January 2010 – Published: 9 February 2010

Correspondence to: C. R. Ellis (cre152@mail.usask.ca)

Published by Copernicus Publications on behalf of the European Geosciences Union.

Abstract

Drawing upon numerous field studies and modelling exercises of snow processes, the Cold Regions Hydrological Model (CRHM) was developed to simulate the four season hydrological cycle in cold regions. CRHM includes modules describing radiative, turbulent and conductive energy exchanges to snow in forest and open environments, as well as provide account for losses from canopy snow sublimation and rain evaporation. Due to the physical-basis and rigorous testing of each module, there is a minimal need for model calibration. To evaluate CRHM, simulations of snow accumulation and melt were compared to observations collected at paired forest and clearing sites of varying latitude, elevation, forest cover density, and climate. Overall, results show that CRHM is capable of characterising the variation of snow accumulation between forest and open sites, achieving a model efficiency of 0.57, with the lowest efficiencies at the forest sites. Simulations of canopy sublimation losses slightly overestimated observed losses from a weighed cut tree, giving a model efficiency of 0.41 for daily losses. Good model performance was demonstrated in simulating energy fluxes to snow at the clearings, but performance was degraded from this under forest canopies due to errors in simulating daily net longwave radiation. However, expressed as cumulative energy to snow over the winter, simulated values were 96% and 98% of that observed at forest and clearing sites, respectively. Overall, good model prediction of the substantial variations in mass and energy between forest and clearing sites suggests that CRHM may be useful as an analytical or predictive tool for snow processes in needleleaf forests.

1 Introduction

Needleleaf forests dominate much of the mountain and boreal regions of the Northern Hemisphere where snowmelt is the most important hydrological event of the year (Gray and Male, 1981). The retention of foliage by evergreen needleleaf tree species during winter acts to decrease snow accumulation via canopy interception losses (Schmidt, 1991; Lundberg and Halldin, 1994; Pomeroy et al., 1998a) and greatly modify energy exchanges to snow (Link and Marks, 1999; Gryning and Batchvarova 2001; Ellis et al., 2010). However, forest cover is often discontinuous, containing clearings of varying dimensions which may differ considerably in snow accumulation (McNay, 1988) and melt characteristics (Metcalfe and Buttle, 1995). As such, management of water derived from forest snowmelt is expected to benefit from the effective prediction of snow accumulation and melt in both forest and open environments.

Forest cover varies in its effects on snow accumulation, with reductions of 30% to 50% of that in nearby clearings observed in cold Canadian and Russian mountain and boreal forests (Pomeroy and Gray, 1995; Pomeroy et al., 2002; Gelfan et al., 2004) to nearly even accumulations reported in temperate Finnish forests (Koivusalo and Kokkonen, 2002). Although numerous mechanisms have been proposed to explain decreased snow accumulations in forests, sublimation of canopy snow has been shown to be the primary factor controlling snow losses to forests (Troendle and King, 1985; Schmidt et al., 1988; Pomeroy and Schmidt, 1993; Lundberg and Halldin, 1994; Parviainen and Pomeroy, 2000). Investigations by Pomeroy and Gray (1995) and Pomeroy et al. (1998a) found that 30 to 45% of annual snowfall in western Canada may be lost by canopy sublimation due to the increased exposure of intercepted snow to the above atmosphere. Consequently, the estimation of canopy sublimation losses have often made appeal to physically-based “ice-sphere” models (e.g. Schmidt, 1991) which adjust sublimation losses from a single, small ice-sphere for the decreased exposure of canopy snow to the atmosphere. Such methods have been shown to well approximate canopy sublimation losses over multiple snowfall events (Pomeroy et al., 1998a) through the coupling of the multi-scale sublimation model to a needleleaf forest interception model (Hedstrom and Pomeroy, 1998).

Alongside interception effects, needleleaf forest cover also influences energy exchanges to snow. The forest layer acts to effectively decouple the above-canopy and sub-canopy atmospheres, resulting in a large suppression of turbulent energy fluxes (Harding and Pomeroy, 1996; Link and Marks, 1999). Consequently, energy to sub-canopy snow is dominated by radiation; itself modified by the canopy through the shading of shortwave irradiance while increasing longwave irradiance from canopy thermal emissions (Link et al., 2004; Sicart et al., 2004; Pomeroy et al., 2009). Forest cover may also affect sub-canopy shortwave radiation by altering snow surface albedo through deposition of forest litter on snow (Hardy et al., 2000; Melloh et al., 2002), or by influencing energy-controlled snow metamorphism rates (Ellis et al., 2010). As such, account for forest effects on energy to snow have largely focused on adjustment of shortwave and longwave fluxes (Hardy et al., 2004; Essery et al., 2008; Pomeroy et al., 2009), although approaches estimating turbulent energy transfer through forests have also been described (Hellström, 2000; Gelfan et al., 2004).

Since the first successful demonstration of snowmelt simulation using an energy-balance approach by Anderson (1976), numerous such snowmelt models have developed (e.g. EBSM, Gray and Landine, 1988; SNTHERM, Jordan, 1991; SHAW, Flerchinger and Saxton, 1989; Snobal, Marks et al., 1999). Due to the differing objective specific to each model, there is considerable variation in the detail to which snow energetics may be described, as well as forcing data and parameterization requirements. In general, more sophisticated snowmelt models possess information requirements that may prohibit their successful employment in more remote environments, where forcing data and parameter information is typically lacking or poorly approximated. Instead, more basic models that maintain a physically-based representation of forest snow processes in cold regions are expected to be better suited in such environments.

Although much focus has been placed on simulating forest snow accumulation and melt processes separately, fewer simulations over the entire snow accumulation and melt period have been demonstrated. As such, this paper outlines and evaluates the simulation of snow accumulation and melt in paired forest and clearing sites of varying forest cover density and climate using the Cold Regions Hydrological Model (CRHM). CRHM is a deterministic model of the hydrological cycle containing process algorithms (modules) developed from field investigations in cold region environments, with modest data and parameter requirements. This paper examines the potential for CRHM to be used to analyze and predict how changes in climate and land-use may affect snow processes in cold region forests.

2 Model description

Described in detail by Pomeroy et al. (2007), CRHM operates through interaction of its four main components: (1) observations, (2) parameters, (3) modules, and (4) variables and states. The description of each component below focuses on the requirements of CRHM for forest environments:

1. Observations: CRHM requires the following meteorological forcing data for each simulation timestep, t (units in []):
   (a) air temperature , T_a [°C];
   (b) humidity, either as vapour pressure, e_a [kPa] or relative humidity, rh [%];
   (c) precipitation, P [$\mathrm{kg\,m^{-2}}\,t^{-1}$];
   (d) wind speed, observed either above, or within the canopy, u [$\mathrm{m\,s^{-1}}$];
   (e) shortwave irradiance, $K\downarrow$ [$\mathrm{W\,m^{-2}}$];
   (f) longwave irradiance, $L\downarrow$ [$\mathrm{W\,m^{-2}}$] (in the absence of observations, $L\downarrow$ may be estimated from T_a and e_a).
2. Parameters: provides a physical description of the site, including latitude, slope and aspect, forest cover density, height, species, and soil properties. In CRHM, forest cover need only be described by an effective leaf area index (LAI‘) and forest height (h); the forest sky view factor (v) may be specified explicitly or estimated from LAI‘. The heights at which meteorological forcing data observations are collected are also specified here.

HESSD
7, 1033–1072, 2010

3. Modules: algorithms implementing the particular hydrological processes are selected here by the user.

4. Initial states and variables: specified within the appropriate module.

2.1 Modules

The following provides an outline of the main modules and associated algorithms in CRHM.

2.1.1 Observation module

To allow for the distribution of meteorological observations away from the point of collection, appropriate corrections are applied to observations within the *observation* module. These include correction of air temperature, humidity, and the amount and phase of precipitation for elevation, as well as correction of shortwave and longwave irradiance for topography.

2.1.2 Snow mass-balance module

In CRHM, snow is conserved within a defined single spatial unit, with changes in mass occurring only through a divergence of incoming and outgoing fluxes. In clearing environments, snow water equivalent (SWE) at the ground may be expressed by the following mass-balance equation of vertical and horizontal snow gains and losses

$$\mathrm{SWE} = \mathrm{SWE}_o + P_s + P_r + H_{\mathrm{in}} - H_{\mathrm{out}} - S - M \tag{1}$$

where SWE_o is the antecedent snow water equivalent [kg m^{-2}], P_s and P_r are the respective snowfall and rainfall rates, H_{in} is the incoming horizontal snow transport, H_{out} is the outgoing horizontal snow transport, S is the sublimation loss, and M is the melt loss [all units kg m^{-2} t^{-1}]. In forest environments Eq. 1 is modified to

$$\mathrm{SWE} = \mathrm{SWE}_o + P_s - (I_s - U_l) + P_r - (I_r - R_d) - M \tag{2}$$

in which I_s is the intercepted snowland, U_l is the addition of sub-canopy snow from canopy unloading, I_r is intercepted snowland, and R_d is the addition of sub-canopy rainfall from canopy drip [all units kg m^{-2} t^{-1}].

The amount of snowfall intercepted by the canopy is dependent on various physical factors, including tree species, forest density, and the antecedent intercepted snowload (L_0). In CRHM, a dynamic canopy snow-balance is calculated, in which the amount of snow interception before canopy unloading is determined by

$$I_s = (I*_s - L_0)\,(1 - e^{-C_l P_s / I*_s}) \tag{3}$$

where C_l is the "canopy-leaf contact area per unit ground" [] and $I*_s$ is the species-specific maximum intercepted snowload [kg m^{-2}], which is determined as a function of the maximum snowload per unit area of branch, $\overline{S}$ [kg m^{-2}], the density of falling snow, ρ_s [kg m^{-3}], and LAI' by

$$I*_s = \overline{S}\left(0.27 + \frac{46}{\rho_s}\right)\text{LAI'}. \tag{4}$$

Sublimation of intercepted snow is estimated following Pomeroy et al.'s (1998) multi-scale model, in which the sublimation rate of intercepted snow, V_i [s^{-1}], is multiplied by the intercepted snowload to give the canopy sublimation flux, q_e [kg m^{-2} s^{-1}], i.e.

$$q_e = V_i I_s. \tag{5}$$

Here, V_i is determined by adjusting the sublimation flux for a 500 µm radius ice-sphere, V_s [s^{-1}], by the intercepted snow exposure coefficient, C_e [], i.e.

$$V_i = V_s C_e, \tag{6}$$

in which C_e was defined by Pomeroy and Schmidt (1993) as

$$C_e = k\left(\frac{I_s}{I_{s*}}\right)^{-F}. \tag{7}$$

where k is a dimensionless coefficient indexing the shape of intercepted snow (i.e. age and structure) and F is the fractal dimension of intercepted snow [~0.4]. The ventilation wind speed of intercepted snow may be set as the measured within-canopy wind speed, or approximated from above-canopy wind speed by

$$u_\xi = u_h e^{-\psi\xi} \tag{8}$$

whereu_ξ [m s^{-1}] is the estimated within-canopy wind speed at the ratio ξ of the entire forest depth [], u_h is the observed wind speed above the canopy [m s^{-1}], and ψ is the canopy wind speed extinction coefficient [] which is determined as a linear function of LAI‘ for various needleleaf species (Eagleson, 2002). Unloading of intercepted snow to the sub-canopy snowpack is calculated as an exponential function of time following Hedstrom and Pomeroy (1998). Additional unloading resulting from melting intercepted snow is estimated by specifying a threshold ice-bulb temperature (T_b) in which all intercepted snow is unloaded when exceeded for three hours.

2.1.3 Rainfall interception and evaporation module

Although the overall focus of this manuscript is that of snow-forest interactions, winter rainfall may represent substantial of water and energy inputs to snow. The fraction of rainfall to sub-canopy snow received as direct throughfall is assumed to be inversely proportional to the fractional horizontal canopy coverage (C_c). All other rainfall is intercepted by the canopy, which may be lost by evaporation (E) or dripped to the sub-canopy upon the canopy rain depth (C) [mm] exceeding the maximum canopy storage depth ($S_{\max}$) [mm]. The intercepted rainload (I_r) [kg m^{-2}] in CRHM is estimated using a simplified Rutter (Rutter, 1971) model approach in which a single storage is determined and is scaled for sparse canopies by C_c (Valente et al., 1997). Evaporation from a fully wetted canopy (E_p) [kg m^{-2}] is calculated using the Penman-Monteith combination equation (Monteith, 1965) for the case of no stomatal resistance, i.e.

$$E = C_c E_p \qquad \text{for} \qquad C = S_{\max}. \tag{9}$$

HESSD

7, 1033–1072, 2010

Simulation of forest snow accumulation and melt

C. R. Ellis et al.

For partially-wetted canopies E is reduced in proportion to the degree of canopy saturation, i.e.

$$E = C_c E_p C / S_{\max} \qquad \text{for} \qquad C < S_{\max}. \tag{10}$$

Rainfall to the sub-canopy is added to the water equivalent of the snowpack. For the case of rainfall to melting snow (i.e. T_s=0 °C) the energy delivered to the snowpack via rainfall advection (Q_p) [MJ m^{-2}] is given by

$$Q_p = 4.2 \times 10^{-3} (P_r - I_r) T_r \tag{11}$$

where T_r is the rainfall temperature [°C] which is approximated by T_a.

2.1.4 Snow energy-balance module

Energy to snow (Q*) is resolved in CRHM as the sum of radiative, turbulent, advective and conductive energy fluxes to snow, i.e.

$$K* + L* + Q_h + Q_e + Q_g + Q_p = \frac{\mathrm{d}U}{\mathrm{d}t} + Q_m = Q* \tag{12}$$

where Q_m is the energy for snowmelt, dU/dt is the change in internal (stored) energy of the snowpack, $K*$ and $L*$ are net shortwave and longwave radiations, respectively, Q_h and Q_e are the net sensible and latent heat turbulent fluxes, respectively, and Q_g is the net ground heat flux [all units MJ m^{-2}]. In Eq. 12, positive magnitudes are considered as energy gains to snow and negative magnitudes as energy losses. Daily melt depth, M [kg m^{-2}] is calculated from Q_m by

$$M = \frac{Q_m}{\rho_w B \lambda_f} \tag{13}$$

where ρ_w is the density of water [kg m^{-3}], λ_f is the latent heat of fusion [MJ kg^{-1}], and B is the fraction of ice in wet snow [0.95–0.97].

Adjustment of energy fluxes to snow for needleleaf forest cover

For the purpose of brevity, the following section outlines the algorithms estimating energy fluxes in forest environments only. For an overview of the procedures for open environments in CRHM, refer to Pomeroy et al. (2007).

Shortwave radiation to forest snow

In CRHM, net shortwave radiation to forest snow ($K*_f$) is equal to the above-canopy irradiance ($K\downarrow$) transmitted through the canopy less the amount reflected from snow, given here by

$$K*_f = K\downarrow \tau(1-\alpha_s) \tag{14}$$

in which α_s is the snow surface albedo [], and τ is the forest shortwave transmittance [], which is estimated using the following variation of Pomeroy and Dion's (1996) formulation (Pomeroy et al., 2009),

$$\tau = e^{-\frac{1.081\cos(\theta)\mathrm{LAI}'}{\sin(\theta)}} \tag{15}$$

where θ is the solar angle above the horizon [radians]. In Eq. 14, the decay of α_s from an initial fresh snow albedo value is approximated as a function of time [days].

Longwave radiation to forest snow

As discussed previously, longwave irradiance to forest snow ($L\downarrow_f$) may be enhanced relative to that in the open as a result of additional thermal emissions from the canopy. Simulation of $L\downarrow_f$ to snow is resolved as the sum of sky and forest longwave emissions, weighted by the sky view factor (v), i.e.

$$L\downarrow_f = vL\downarrow + (1-v)\varepsilon_f \sigma T_f^4. \tag{16}$$

Here, ε_f is the forest thermal emissivity [], σ is the Stefan-Boltzmann constant [$\mathrm{W\,m^{-2}\,K^{-4}}$], and T_f is the forest temperature [K]. Longwave exitance from snow ($L\uparrow$) is determined by

$$L\uparrow = \varepsilon_s \sigma T_s^4 \tag{17}$$

where ε_s is the emissivity of snow [0.98], and T_s is the snow surface temperature [K] which is resolved following the longwave psychrometric approach developed by Pomeroy (2010)

$$T_s = T_a + \frac{\varepsilon\left(L\downarrow - \sigma T_a^4\right) + \lambda_v (e_a - e_s)\rho_a / r_a}{\varepsilon\sigma T_a^3 + (c_p + \lambda_v \Delta)\rho_a / r_a} \tag{18}$$

where ε is the thermal emissivity of the atmosphere [], e_a and e_s are the respective observed and saturation vapour pressures [kPa], c_p is the specific heat capacity of air [$\mathrm{KJ\,kg^{-1}\,K^{-1}}$], λ_v is the latent heat of vapourization [$2501\,\mathrm{kJ\,kg^{-1}}$ at 0 °C], r_a is the aerodynamic resistance [$\mathrm{s\,m^{-1}}$], and Δ is the slope of the saturation vapour pressure curve [$\mathrm{kPa\,K^{-1}}$].

Sensible (Q_h) and latent (Q_e) heat fluxes

Determination of Q_h and Q_e in the open and forest sites are made using the semi-empirical formulations developed by Gray and Landine (1988)

$$Q_h = -0.92 + 0.076 u_{\mathrm{mean}} + 0.19 T_{\mathrm{max}} \tag{19}$$

$$Q_e = 0.08(0.18 + 0.098 u_{\mathrm{mean}})(6.11 - 10 ea_{\mathrm{mean}}) \tag{20}$$

where u_{mean} is the mean daily wind speed [$\mathrm{m\,s^{-1}}$], T_{max} is the maximum daily air temperature [°C], and ea_{mean} is the mean daily vapour pressure [kPa]. The primary mass and energy balance calculation routines for both forest and clearing environments within CRHM are summarized in Fig. 1.

3 Model application

Simulations of snow accumulation and melt using CRHM were performed at five paired clearing and forest environments of varying location, climate, forest species, and forest cover density. With the exception of the Marmot Creek sites, all simulations were performed as part of the second snow model inter-comparison project (SnoMIP2) (Rutter et al., 2009; Essery et al., 2009). This initiative involved the off-line simulation of snow accumulation and melt in paired forest and nearby clearing sites located in Canada, Switzerland, Finland, Japan and the United States. Hourly standard meteorological forcing data, site descriptions, and initial states were provided to each participant by the SnoMIP2 facilitators. All simulations in SnowMIP2 were executed "blindly" with the exception of the Switzerland location for the 2002-03 season where SWE field data were provided to allow for the option of model calibration. Location, topography and forest cover descriptions for all sites are given in Table 1, and site pictures in Fig. 2. Simulations of snow accumulation and melt were performed for both forest and adjacent forest clearing sites at each location for the period ranging from 1 October to approximately 1 June. For each simulation timestep, appropriate energy-balance, mass-balance, and state variables were outputted by the model.

4 Simulation of snow accumulation and melt

4.1 Evaluation of model performance

Simulations of snow accumulation and melt by CRHM were evaluated in terms of the accuracy of representing:

1. the variation in mean and maximum seasonal SWE observed at all sites; and
2. the timing and quantity of SWE accumulation and melt at individual sites.

For *i* and *ii* above, model performance was assessed by the following three measures: the mean model bias (MB) index, the model efficiency (ME) index, and the root mean square difference (RMSE). These indexes were used as they provide a rather complementary evaluation of model performance, with the MB comparing the total simulation output to the total of observations, the ME an indication of model performance compared to the mean of the observations, and the RMSE a quantification of the absolute amount of unit error between simulations and observations. Here, the MB is calculated as

$$\mathrm{MB} = \frac{1}{n}\sum_{i=1}^{n}(x_{\mathrm{sim}} - x_{\mathrm{obs}}) \quad (21)$$

where x_{sim} and x_{obs} are the simulated and observed values at a given timestep for n number of paired simulated and observed values. Accordingly, MB values less than 1 signify an overall under-prediction by the model and values greater that 1 an overall over-prediction by the model. The model efficiency (ME) index is given by

$$\mathrm{ME} = 1 - \left[\frac{\sum_{i=1}^{n}(x_{\mathrm{sim}} - x_{\mathrm{obs}})^2}{\sum_{i=1}^{n}(x_{\mathrm{obs}} - x_{\mathrm{avg}})^2}\right] \quad (22)$$

where x_{avg} is the mean value of n observations. Accordingly, model efficiency increases as the ME index approaches 1, which represents a perfect match between simulations and observations; 0 indicates an equal efficiency between simulations and the x_{avg}, with increasingly negative values signifying a progressively superior estimation by the x_{avg}. The root mean square error (RMSE) is determined by

$$\mathrm{RMSE} = \sqrt{\frac{1}{n}\sum_{i=1}^{n}(x_{\mathrm{sim}} - x_{\mathrm{obs}})^2} \quad (23)$$

4.1.1 Simulation of mean and maximum winter SWE at all sites

Amongst all sites, considerable variation in mean and maximum seasonal SWE was observed, with mean SWE ranging from 20 to 160 kg m^{-2}, and maximum SWE from 29 to 295 kg m^{-2}. Large variations in SWE were also observed between paired forest and clearings, with forest accumulations ranging from 30% of the clearing accumulation at the Alptal location (2003–04) to approximately even accumulations at the BERMS location.

Simulated and observed mean and maximum SWE at all sites are shown in Fig. 3. Here, simulations exhibit a small systematic under-prediction of mean SWE for all sites (MB=0.97), with a slightly greater under-prediction for the forest sites (Table 2). In comparison, a greater under-prediction of maximum SWE at all sites was realised (MB=0.94). However, the high ME value indicates CRHM well represented the variability in mean and maximum SWE accumulations between sites. Similar to MB results, the ME shows superior prediction of mean SWE to that of maximum SWE, as well as better prediction for clearing sites relative to forest sites. However, due to less snow at the forest sites, the lower MB and ME indexes at the forest sites translate into similar magnitudes of absolute error to that at the clearing sites (RMSE=∼16 kg m^{-2}), and even lower absolute errors in the prediction of forest maximum SWE.

4.1.2 Simulation of winter SWE accumulation and melt at individual sites

Simulations of snow accumulation and melt at individual sites exhibited considerable variation in the accuracy of predicting the quantity and timing of SWE. However, as seen in Fig. 4, model simulations are able to capture the general differences in the timing of accumulation and melt between paired forest clearing sites. Model performance indices for all simulations at individual sites, as well as the mean indices for forest and clearing sites are given in Table 3. Here, a slight systematic underestimation of forest SWE is realised (MB=0.92), with no bias for the simulation of SWE at the clearing sites (MB=1.0). The mean ME for SWE simulations at individual sites was 0.57, with slightly higher efficiencies at the clearing sites. For individual simulations, highest and lowest ME were both obtained at the Alptal forest site, with ME values of 0.93 and −0.03 for the of 2002–03 and 2003–04 periods, respectively. Overall, the mean absolute error for all sites was 26.5 $kg\,m^{-2}$, with higher mean absolute errors realised for the clearing sites.

Due to the discontinuity of SWE observations over the winter at each site, exact determinations of the start, peak and end of snow accumulation were not possible. Alternatively, an evaluation of the timing of snow accumulation was provided by determination of the MB, ME, and RMSE of simulated SWE at the first, last and maximum SWE observation at each site (Table 4). Results show for the first observation, SWE is slightly over-predicted at the clearing sites (MB=1.07), with a large under-prediction of forest SWE (MB=0.6). At maximum SWE, little systematic simulation bias occurs for SWE simulations at all sites (MB=0.99); a result of the slight over-prediction and under-prediction at the clearing and forest sites, respectively. For the last observed SWE, the high MB values indicate a large over-estimation of SWE at the end of melt, suggesting a substantial lag in simulated snow depletion. Poor simulation of late-season SWE is also reflected in the low ME and high RMSE as compared to the first and maximum observations.

4.2 Simulation of canopy sublimation

The above results show CRHM is generally able to represent the observed differences in snow accumulation between paired forest and clearing sites. Considering that these differences are largely the result of canopy sublimation losses, model performance in estimating canopy sublimation is further investigated here. Evaluation of canopy sublimation was performed using canopy snowload measurements from a spruce tree suspended from a load cell at the Marmot Creek spruce forest site. Changing tree weight was correlated to the intercepted snowload by the measured difference of snow accumulations between the forest and adjacent clearing site (Hedstrom and Pomeroy, 1998). Changes in tree tare resulting from desiccation and needle loss were also accounted for, as was snow unloading from the canopy by measurements of snow collected in three lysimeters suspended under the canopy. Simulation of canopy sublimation was performed for the period of 14 January to 3 March, using precipitation and incoming radiation data from an adjacent clearing and within-canopy wind speed and humidity measured at the suspended tree.

Over the period, approximately one-half of snowfall was lost by canopy sublimation, with respective mean daily observed and simulated losses of 0.52 kg m^{-2} and 0.55 kg m^{-2}, giving corresponding MB values of 1.06 and a ME of 0.41. The time-series of hourly canopy sublimation losses in Fig. 5 (top) shows a general agreement between observed and simulated values, with higher rates corresponding to periods of relatively high wind speeds and low relative humidity (Fig. 5, bottom). Overall, the cumulative amounts of observed and simulated sublimation were similar, with total losses of approximately 24 and 26 kg m^{-2} for the period, respectively.

5 Simulation of energy fluxes to snow

To investigate CRHM's handling of energy fluxes, simulations of energy fluxes to snow were compared to measurements made at the Marmot Creek paired pine forest and clearing sites. Measurements from these sites include incoming and outgoing shortwave and longwave radiation, as well as ground heat fluxes. However, as no direct measures of sensible and latent heat were made, evaluation of the simulation of these fluxes was not possible.

Time-series plots of observed and simulated energy terms during snowcover in Fig. 6 and model indices in Table 5 show a good agreement for all shortwave radiation terms at forest and clearing sites, and good prediction of L^* at the clearing site. However, despite the good prediction of the individual incoming and outgoing longwave fluxes ($L\downarrow$ and $L\uparrow$) at the forest, the prediction of forest net longwave radiation (L^*) was poor, which contributed in degrading estimates of total net radiation to snow ($Q_n = K^* + L^*$). Despite the large errors in estimating the ground energy flux (Q_g) at clearing and forest sites, little effect on overall model performance resulted due to the small contribution of Q_g to total energy (note that no energy to snow from rainfall, Q_p, was observed nor simulated). In terms of systematic bias, the small negative and positive values of L^*, Q_n andQ_g observed (and simulated) provided MB values that were often misleading and not instructive to model assessment. Alternatively, the systematic model bias of energy terms was calculated as the difference between mean simulated and observed values. Here, the offsetting of small negative and positive biases of individual energy terms resulted in the relatively low bias errors at the forest and clearing sites of −0.37 and −0.59 W m^{-2}, respectively. The close comparison of simulated and observed energy terms in Fig. 7 demonstrate that CRHM was able to characterise the substantial difference between clearing and forest energy balances, and provide a good estimation of total energy to snow. Also shown in Fig. 7 are the simulated sensible and latent energy totals, which were greater in absolute magnitude at the clearing to that of the forest, but provided approximately equal contributions relative to total energy to snow (Q^*) at both sites.

6 Discussion and conclusions

Overall, results show that CRHM is able to accurately simulate the quantity and timing of snow accumulation and melt under needleleaf forest cover and forest clearings. Good results were obtained both in terms of simulating the variation in snow accumulation between paired forest and clearing sites, and also in the simulation of the timing and quantity of snow accumulation and melt at individual sites. The accurate representation of the major energy terms between the pine forest and clearing sites suggests that despite modest data requirements, the physical basis of the model is sufficient for representing forest-snow processes in environments of varying forest cover and meteorology.

Simulations of mean and maximum seasonal SWE exhibited little systematic bias over forest sites, clearing sites, or all sites. This suggests that much of the errors incurred to be random in nature, resulting either from errors in observations or model errors. For simulations of SWE at individual sites, errors also appear to be random rather than systematic, considering that the best and worst model efficiencies were obtained for the same site over consecutive winters (i.e. Alptal forest). In all, the poorest model efficiencies of SWE were achieved at the 2003–04 Alptal forest and Marmot pine sites, which had substantially lower snowfall relative to the other sites. Such results may be expected as shallower snowpacks would be more sensitive to simulation errors in mass and energy, thus resulting in larger relative errors. Notwithstanding these limitations, encouraging simulation results were obtained, as exemplified in the good representation of the extreme differences in the relative snow accumulation between the forest and clearing observed for the two winter periods at the Alptal location.

Although good prediction of SWE was made for the start and peak of accumulation, poorer predictions were made at the end of accumulation, suggesting a lag in simulated melt rates. Particularly large lags in simulated snow depletion occur at the Alptal (2003–04) and Marmot spruce clearing sites, where the substantial late-season snowfall may have resulted in an overestimation of the additional energy deficit to the snowpack. Accordingly, improvement in CRHM's representation of snowmelt timing and rate may require addressing the handling of internal snow energetics subsequent to large snowfalls.

Compared to observations of snow load change from a suspended tree, satisfactory model simulation of canopy sublimation was achieved both in terms of daily and cumulative losses. The correspondence of periods of high sublimation with relatively high wind speeds and low relative humidity demonstrate the physically-based manner in which canopy sublimation is accounted for by CRHM. Accordingly, such approaches are likely necessary to predict the large differences in accumulation which may occur between forest and clearings resulting from variations in forest cover density and climate. However, sensitivity analysis has shown the sublimation module in CRHM to be very sensitive to errors in the intercepted snowload, which may have been brought about by the simplistic approach in handling canopy unloading in CRHM. Consequently, increased confidence in the model's representation of canopy sublimation losses would likely by gained through better understanding the processes controlling canopy unloading of snow.

Although simulations of energy fluxes were evaluated against observations at only a single paired forest and clearing site, results show the model able to well represent both the total energy to snow and the relative contributions of individual energy terms. All errors in estimating shortwave and longwave radiation were small and below the measurement error of the radiometers used in their measurement. However, the presence of canopy cover is seen to dramatically decrease the model's predictive capability for net radiation and total energy to snow, as seen in the decreasing model efficiency indexes with the increasing number of combined energy terms. Yet, cumulative errors in estimating total energy to snow were relatively modest, owing in part to the error cancellation of individual energy terms. Although no evaluation of sensible and latent energy terms was performed, simulated magnitudes were similar to those observed in cold-region needleleaf forest environments by Harding and Pomeroy (1996) and estimated by Pomeroy and Granger (1997).

Despite some uncertainly in model performance, results show CRHM is able to provide good estimation of critical forest-snow processes in environments of highly variable forest cover and climate, and with only modest requirements for site information and forcing data. As simulations were performed without calibration to any objective function, there is increased confidence that CRHM is capable of representing the effects on snow accumulation and melt brought about by changes in forest cover or climate. Consequently, results from this model evaluation provide encouragement for the use of CRHM as a diagnostic or predictive tool for investigating needleleaf forest cover effects on snow processes in cold regions.

Appendix A

Notation

B	fraction of ice in snow []
C	degrees Celsius [°]
C_c	fraction of horizontal canopy coverage []
C_e	intercepted snow exposure coefficient []
C_l	"canopy-leaf contact area" per unit ground []
c_p	specific heat capacity of air [$\mathrm{kJ\,kg^{-1}\,K^{-1}}$]
E	evaporation from a partially wetted canopy [$\mathrm{kg\,m^{-2}}$]
E_p	evaporation from a fully wetted canopy [$\mathrm{kg\,m^{-2}}$]
e_a	vapour pressure [kPa]
ea_{mean}	daily mean vapour pressure [kPa]
e_s	saturation vapour pressure [kPa]
F	fractal dimension (of intercepted snow) []
h	forest height [m]
H_{in}	incoming horizontal snow transport [$\mathrm{kg\,m^{-2}}\,t^{-1}$]
H_{out}	outgoing horizontal snow transport [$\mathrm{kg\,m^{-2}}\,t^{-1}$]
I_r	canopy intercepted rainload [$\mathrm{kg\,m^{-2}}$]
I_s	canopy intercepted snowload [$\mathrm{kg\,m^{-2}}$]
$I{*}_s$	the species specific maximum intercepted snowload [$\mathrm{kg\,m^{-2}}$]
k	intercepted snow shape coefficient []
K	degrees Kelvin []
$K{\downarrow}$	shortwave irradiance [$\mathrm{MJ\,m^{-2}}$ or $\mathrm{W\,m^{-2}}$]
$K{\downarrow}_f$	sub-canopy shortwave irradiance [$\mathrm{MJ\,m^{-2}}$ or $\mathrm{W\,m^{-2}}$]
$K{\uparrow}_f$	reflected sub-canopy shortwave irradiance [$\mathrm{W\,m^{-2}}$]
$K{*}$	net shortwave radiation [$\mathrm{MJ\,m^{-2}}$ or $\mathrm{W\,m^{-2}}$]

HESSD
7, 1033–1072, 2010
Simulation of forest snow accumulation and melt
C. R. Ellis et al.

$K*_f$	sub-canopy net shortwave radiation [MJ m^{-2} or W m^{-2}]
$L\downarrow$	longwave irradiance [MJ m^{-2} or W m^{-2}]
$L\downarrow_f$	sub-canopy longwave irradiance [MJ m^{-2} or W m^{-2}]
$L\uparrow$	surface longwave exitance [MJ m^{-2} or W m^{-2}]
$L\uparrow_f$	sub-canopy surface longwave exitance [MJ m^{-2} or W m^{-2}]
$L*$	net longwave radiation [MJ m^{-2} or W m^{-2}]
$L*_f$	sub-canopy net longwave radiation [MJ m^{-2} or W m^{-2}]
LAI'	effective leaf area index []
M	snowmelt [kg m^{-2} t^{-1}]
MB	model bias index []
ME	model efficiency index []
P	precipitation [kg m^{-2} t^{-1}]
P_s	snowfall [kg m^{-2} t^{-1}]
P_r	rainfall [kg m^{-2} t^{-1}]
q_e	canopy sublimation rate [kg m^{-2} s^{-1}]
Q_e	net latent heat flux [MJ m^{-2} or W m^{-2}]
Q_h	net sensible heat flux [MJ m^{-2} or W m^{-2}]
Q_m	melt energy [MJ m^{-2} or W m^{-2}]
Q_n	net radiationto snow [MJ m^{-2} or W m^{-2}]
Q_{nf}	net radiation to forest snow [MJ m^{-2} or W m^{-2}]
Q_p	net energy advected to snow by precipitation [MJ m^{-2} or W m^{-2}]
Q_g	net ground heat flux [MJ m^{-2} or W m^{-2}]
Q^*	net energy to snow [MJ m^{-2} or W m^{-2}]
r_a	aerodynamic resistance [s m^{-1}]
rh	relative humidity [%]
R_d	canopy drip [kg m^{-2} t^{-1}]

HESSD
7, 1033–1072, 2010

Simulation of forest snow accumulation and melt

C. R. Ellis et al.

RMSE	root mean square error [units variable]
S	sublimation [kg SWE m^{-2} t^{-1}]
$\overline{S}$	maximum snowload per unit area of branch [kg m^{-2}]
SWE	snow water equivalent [kg m^{-2}]
SWE_o	antecedent snow water equivalent [kg m^{-2}]
t	timestep
T_a	air temperature [°C or K]
T_b	threshold ice-bulb temperature for snow unloading [°C]
T_f	forest temperature [K]
T_r	rainfall temperature [°C]
T_{max}	maximum daily air temperature [°C]
V_i	sublimation rate of intercepted snow [s^{-1}]
u	wind speed [m s^{-1}]
u_{mean}	mean daily wind speed [m s^{-1}]
u_ξ	within-canopy wind speed at depth ξ from canopy top [m s^{-1}]
u_h	wind speed at canopy top [m s^{-1}]
U	internal (stored) snow energy [MJ m^{-2}]
U_l	snow unloading from canopy [kg m^{-2}]
x_{avg}	mean observed value []
x_{obs}	observed value []
x_{sim}	simulated value []
τ	forest shortwave transmittance []
α_s	snow albedo []
λ_f	latent heat of fusion [MJ kg^{-1}]
λ_v	latent heat of sublimation [MJ kg^{-1}]
Δ	slope of saturation vapour pressure curve [kPa K]
ε_f	emissivity of forest canopy []

HESSD

7, 1033–1072, 2010

Simulation of forest snow accumulation and melt

C. R. Ellis et al.

ε_s emissivity of snow []
ψ wind speed canopy extinction coefficient []
θ solar elevation angle [radians]
σ Stefan-Boltzmann constant [$W\,m^{-2}\,K^{-4}$]
ρ_a density of air [$kg\,m^{-3}$]
ρ_s density of snowfall [$kg\,m^{-3}$]
ρ_w density of water [$kg\,m^{-3}$]
v sky view factor []
ξ depth from canopy top (as a fraction of forest height) []

Acknowledgements. The authors would like to thank R. Essery and N. Rutter for their efforts in facilitating the SnoMIP2 initiative, which provided an invaluable opportunity for model evaluation and improvement. Funding and support was provided by the Natural Sciences and Engineering Research Council of Canada Alexander Graham Bell Doctoral and Michael Smith Foreign Student Supplement scholarships, the Canada Research Chairs Program, the Canada Foundation for Innovation (CFI), the Natural Environment Research Council (UK), the GEWEX Americas Prediction Project (GAPP), and the Biogeosciences Institute, University of Calgary.

References

Anderson, E. A.: A point energy and mass balance model of a snow cover. NWS Technical Report 19, National Oceanic and Atmospheric Administration, Washington, DC, 150 pp., 1976.

Eagleson, P. S.: Ecohydrology, Darwinian expression of vegetation form and function, Cambridge University Press, Cambridge, UK, 443 pp., 2002.

Ellis, C., Pomeroy, J., Essery, R., and Link, T.: Effects of needleleaf forest cover on radiation for snowmelt in the Canadian Rocky Mountains, Can. J. Forest Res., in preparation, 2010.

Essery, R., Rutter, N., Pomeroy, J., Baxter, R., Stähli, R., Gustafsson, D., Barr, A., Bartlett, P., and Elder, K.: An evaluation of forest snow process simulations. B. Am. Meteorol. Soc., 90 (8), 1120–1135, 2009.

Essery, R. L. H., Pomeroy, J. W., Ellis, C., and Link, T.: Modelling longwave radiation to snow beneath forest canopies using hemispherical photography and linear regression, Hydrol. Process., 22, 2788–2800, doi:10.1002/hyp.6630., 2008.
Flerchinger, G. N. and Saxton, K. E.: Simultaneous heat and water model of a freezing snow-residue-soil system I. Theory and development, T. ASAE, 32(2), 565–571, 1989.
Gelfan, A., Pomeroy, J. W., and Kuchment, L.: Modelling forest cover influences on snow accumulation, sublimation and melt, J. Hydrometeorol., 5, 785–803, 2004.
Gray, D. M. and Male, D. H.: Handbook of Snow: Principles, Processes, Management and Use, Pergamon Press, Toronto, 776 pp., 1981.
Gray, D. M. and Landine, P. G.: An energy budget snowmelt model for the Canadian Prairies, Can. J. Earth Sci., 22(3), 464–472, 1988.
Gryning, S. and Batchvarova, E.: Energy balance of a sparse coniferous high-latitude forest under winter conditions, Bound-Lay. Meteorol., 99, 465–488, 2001.
Harding, R. J. and Pomeroy, J. W.: The energy balance of the winter boreal landscape, J. Climate, 9, 2778–2787, 1996.
Hardy, J. P., Melloh, R., Robinson, P., and Jordan, R.: Incorporating effects of forest litter in a snow process model, Hydrol. Process., 14, 3227–3237, 2000.
Hardy, J., Melloh, R., Koenig, G., Marks, D., Winstral, A., Pomeroy, J., and Link, T.: Shortwave radiation transmission through conifer canopies, Agr. Forest Meteorol., 126, 257–270, 2004.
Hedstrom, N. R. and Pomeroy, J. W.: Measurements and modelling of snow interception in the boreal forest, Hydrol. Process., 12, 1611–1625, 1998.
Hellström, R. Å.: Forest cover algorithms for estimating meteorological forcing in a numerical snow model, Hydrol. Process., Special Issue: Eastern Snow Conference, 14(18), 3239–3256, 2000.
Jordan, R.: A one-dimensional temperature model for a snow cover, Technical documentation for SNTHERM.89, US Army Corps of Engineers Cold Regions Research and Engineering Laboratory, Special Report 91–16, Hanover, New Hampshire, 49 pp., 1991.
Koivusalo, H. and Kokkonen, T.: Snow processes in a forest clearing and in a coniferous forest, J. Hydrol., 262, 145–164, 2002.
Link, T. E. and Marks, D.: Point simulation of seasonal snow cover dynamics beneath boreal forest canopies, J. Geophys. Res., 104, 27841–27857, 1999.
Link, T. E., Marks, D., and Hardy, J.: A deterministic method to characterize canopy radiative transfer properties, Hydrol. Process., 18, 3583–3594, 2004.

Lundberg, A. and Halldin, S.: Evaporation of intercepted snow, analysis of governing factors, Water Resour. Res., 30, 2587–2598, 1994.

Marks, D., Domingo, J., Susong, D., Link, T., and Garen, D.: A spatially distributed energy balance snowmelt model for application in mountain basins Hydrol. Process., 13, 1935–1959, 1999.

McNay, R. S., Petersen, L. D., and Nyberg, J. B.: The influence of forest stand characteristics on snow interception in the coastal forests of British Columbia. Can. J. Forest Res., 18, 566–573, 1988.

Melloh, R. A., Hardy, J. P., Bailey, R. N., and Hall, T. J.: An efficient snow albedo model for the open and sub-canopy, Hydrol. Process., 16, 3571–3584, 2002.

Metcalfe, R. A. and Buttle, J. M.: Controls of canopy structure on snowmelt rates in the boreal forest, Proceedings of the 52nd Eastern Snow Conference, 249–257, 1995.

Monteith, J. L.: Evaporation and environment, Sym. Soc. Exp. Biol., 19, 205–234, 1965.

Parviainen, J. and Pomeroy, J. W.: Multiple-scale modelling of forest snow sublimation, initial findings, Hydrol. Process., 14, 2669–2681, 2000.

Pomeroy, J. W. and Schmidt, R. A.: The Use of Fractal Geometry in Modelling Intercepted Snow Accumulation and Sublimation, Proceedings of the Eastern Snow Conference, 50, 1–10, 1993.

Pomeroy, J. W. and Gray, D. M.: Snowcover Accumulation, Relocation and Management. NHRI Science Report No. 7, National Hydrology Research Institute, Environment Canada, Saskatoon, SK, 134 pp., 1995.

Pomeroy, J. W. and Dion, K.: Winter radiation extinction and reflection in a boreal pine canopy, measurements and modelling, Hydrol. Process., 10, 1591–1608, 1996.

Pomeroy, J. W. and Granger, R. J.: 1997. Sustainability of the western Canadian boreal forest under changing hydrological conditions - I- snow accumulation and ablation, in: Sustainability of Water Resources under Increasing Uncertainty, edited by: Rosjberg, D., Boutayeb, N., Gustard, A., Kundzewicz, Z., and Rasmussen, P., IAHS Publ No. 240, IAHS Press, Wallingford, UK, 237–242, 1997.

Pomeroy, J. W., Parviainen, J., Hedstrom, N., and Gray, D. M.: Coupled modelling of forest snow interception and sublimation, Hydrol. Process., 12, 2317–2337, 1998a.

Pomeroy, J. W., Gray, D. M., Hedstrom, N. R., and Janowicz, J. R: Prediction of seasonal snow accumulation in cold climate forests, Hydrol. Process., 16, 3543–3558, 2002.

Pomeroy, J. W., Gray, D. M., Brown, T., Hedstrom, N. R., Quinton, W. L., Granger, R. J., and Carey, S. K.: The cold regions hydrological model, a platform for basing process representation and model structure on physical evidence, Hydrol. Process., 21(19), 2650–2667, 2007.

Pomeroy, J. W., Marks, D., Link, T., Ellis, C., Hardy, J., Rowlands, A., and Granger, R.: The impact of coniferous forest temperature on incoming longwave radiation to melting snow, Hydrol. Process., 23(17), 2513–2525, doi:10.1002/hyp.7325, 2009.

Rutter, A. J., Kershaw, K. A., Robins, P. C., and Morton, A. J.: A predictive model of rainfall interception in forests. I. Derivation of the model from observations in a plantation of Corsian pine, Agr. Meteorol., 9, 367–384, 1971.

Rutter, N., Essery, R., Pomeroy, J., Altimir, N., Andreadis, K., Baker, I., Barr, A., Bartlett, P., Boone, A., Deng, H., Douville, H., Dutra, E., Elder, K., Ellis, C., Feng, X., Gelfan, A., Goodbody, A., Gusev, Y., Gustafsson, D., Hellstrom, R., Hirabayashi, Y., Hirota, T., Jonas, T., Koren, V., Kuragina, A., Lettenmaier, D., Li, W-P, Martin, E., Nasanova, O., Pumpanen, J., Pyles, R., Samuelsson, P., Sandells, M., Schadler, G., Shmakin, A., Smirnova, T., Stahli, M., Stockli, R., Strasser, U., Su, H., Suzuki, K., Takata, K., Tanaka, K., Thompson, E., Vesala, T., Viterbo, P., Wiltshire, A., Xia, K., Xue, Y., and Yamazaki, T.: Evaluation of forest snow process models (SnowMip2), J. Geophys. Res.-Atmos., 114, D06111, doi:10.1029/2008JD011063, 2009.

Schmidt, R. A., Jairell, R. L., and Pomeroy, J. W.: Measuring snow interception and loss from an artificial conifer, P. West. Snow Conf., 56, 166–169, 1988.

Schmidt, R. A.: Sublimation of snow by an artificial conifer, Agr. Forest Meteorol., 54, 1–27, 1991.

Schmidt, R. A., Troendle, C. A., and Meiman, J. R.: Sublimation of snowpacks in subalpine conifer forests, Can. J. Forest Res., 28, 501–513, 1998.

Sicart, J. E., Pomeroy, J. W., Essery, R. L. H., Hardy, J. E., Link, T., and Marks, D.: A sensitivity study of daytime net radiation during snowmelt to forest canopy and atmospheric conditions, J. Hydrometeorol., 5, 744–784, 2004.

Troendle, C. A. and King, R. M.: The effect of timber harvest on the Fool Creek watershed: 30 years later, Water Resour. Res., 21, 1915–1922, 1985.

Valente, F., David, J. S., and Gash, J. H. C.: Modelling interception loss for two sparse eucalypt and pine forests in central Portugal using reformulated Rutter and Gash analytical models, J. Hydrol., 190, 141–162, 1997.

Table 1. Location, topography, and forest cover descriptions of paired open and forest sites used in simulations of snow accumulation and melt.

Site	Years	Latitude	Elevation	Slope, aspect	Height, species	LAI'	v
Alptal, Switzerland Switzerland (forest)	2002–04	47°3′ N	1185 m	3° W	25 m spruce and fir	2.5	0.04
Alptal, Switzerland (clearing)	2002–04	47°3′ N	1220 m	11° W	–	–	–
BERMS, Saskatchewan, Canada (forest)	2002–03	53°55′ N	579 m	level	12–15 m jack pine	1.66	0.28
BERMS, Saskatchewan, Canada (clearing)	2002–03	53°57′ N	579 m	level	–	–	–
Fraser, Colorado, USA (forest)	2003–05	39°53′ N	2820 m	17°, 305°	~27 m pine, spruce/ fir	3	not given
Fraser, Colorado, USA (clearing)	2003–05	39°53′ N	2820 m	17°, 305°	2–4 m sparse trees	0.4	not given
Marmot Creek, Alberta, Canada (pine forest)	2007–08	50°56′ N	1500 m	level	~15 m lodgepole pine	1.5	0.20
Marmot Creek, Alberta, Canada (pine clearing)	2007–08	50°56′ N	1430 m	level	–	–	–
Marmot Creek, Alberta, Canada (spruce forest)	2007–08	50∘56′ N	1850 m	level	17–20 m Engelmann spruce	2.0	0.15
Marmot Creek, Alberta, Canada (spruce clearing)	2007–08	50°56′ N	1850 m	level	–	–	–

HESSD

7, 1033–1072, 2010

Table 2. Model bias index (MB), model efficiency index (ME), and root mean square error (RMSE) of simulated mean and maximum snow water equivalent (SWE) for clearing sites, forest sites, and all sites.

	Mean SWE [$kg\,m^{-2}$]			Maximum SWE [$kg\,m^{-2}$]		
	Clearing	Forest	All	Clearing	Forest	All
Model bias (MB)	0.99	0.95	0.97	0.94	0.94	0.94
Model efficiency (ME)	0.97	0.93	0.96	0.92	0.87	0.90
Root mean square error (RMSE)	16.0	16.1	15.8	27	21.6	24.4

Table 3. Determined model bias index (MB), model efficiency index (ME), and root mean square error (RMSE) for simulations of snow water equivalent (SWE) at individual sites.

Site	MB []	ME []	RMSE [kg SWE m^{-2}]
Alptal 2002–03 (clearing)	0.87	0.88	35.6
Alptal 2002–03 (forest)	0.99	0.93	17.6
Alptal 2003–04 (clearing)	1.20	0.64	51.1
Alptal 2003–04 (forest)	0.65	−0.03	25.9
BERMS 2002–03 (clearing)	1.10	0.70	12.6
BERMS 2002–03 (forest)	1.20	0.63	12.9
Fraser 2003–04 (clearing)	1.10	0.32	37.8
Fraser 2003–04 (forest)	0.70	0.45	40.3
Fraser 2004–05 (clearing)	1.10	0.32	37.8
Fraser 2004–05 (forest)	0.70	0.45	40.3
Marmot 2007–08 (pine clearing)	0.90	0.43	13.0
Marmot 2007–08 (pine forest)	1.09	0.13	9.50
Marmot 2007–08 (spruce clearing)	0.80	0.58	28.0
Marmot 2007–08 (spruce forest)	1.10	0.70	8.80
Forest sites (mean)	0.94	0.47	22.2
Clearing Sites (mean)	1.00	0.54	29.7
All sites (mean)	0.96	0.51	26.5

HESSD

7, 1033–1072, 2010

Table 4. Determined model bias index (MB), model efficiency index (ME) and root mean square error (RMSE) for simulations of SWE at the first SWE observation, maximum SWE observation, and last SWE observation.

	SWE at first observation			At maximum observed SWE			SWE at last observation		
	Clearing	Forest	All	Clearing	Forest	All	Clearing	Forest	All
MB	1.07	0.60	0.89	1.08	0.95	0.99	3.85	3.59	3.64
ME	0.96	0.91	0.93	0.87	0.89	0.88	−3.50	−5.97	−5.70
RMSE	12.4	5.8	9.8	30.9	22.6	27.0	66.4	18.9	48.8

HESSD

7, 1033–1072, 2010

Simulation of forest snow accumulation and melt

C. R. Ellis et al.

Table 5. Model efficiency index (ME), root mean square error (RMSE), and the difference between mean simulated and observed values of: shortwave irradiance ($K\downarrow$), reflected shortwave ($K\uparrow$), net shortwave radiation ($K*$), longwave irradiance ($L\downarrow$), longwave exitance ($L\uparrow$), net longwave radiation ($L*$), net radiation (Q_n), net ground heat flux (Q_g), and total energy to snow ($Q*$) (i.e. $Q*=Q_m+\mathrm{d}U/\mathrm{d}t$) for pine forest and clearing sites.

Site	$K\downarrow$	$K\uparrow$	$K*$	$L\downarrow$	$L\uparrow$	$L*$	Q_n	Q_g	$Q*$[1]
ME (Clearing)	–	0.94	0.94	–	0.82	0.67	0.80	−0.92	0.78
ME (Forest)	0.87	0.82	0.83	0.90	0.79	0.08	0.27	−2.77	0.25
RMSE (Clearing)	–	13.9	13.9	–	18.2	18.2	22.4	1.8	23.1
RMSE (Forest)	6.1	5.3	2.7	9.24	13.1	8.56	9.08	2.2	9.64
Mean simulated – mean observed (Clearing)	–	2.75	−2.75	–	−3.15	3.15	0.40	−0.03	−0.37
Mean simulated – mean observed (Forest)	0.36	−0.02	0.38	−2.70	−1.70	−1.0	−0.60	0.02	−0.59

[1] excluding sensible and latent fluxes

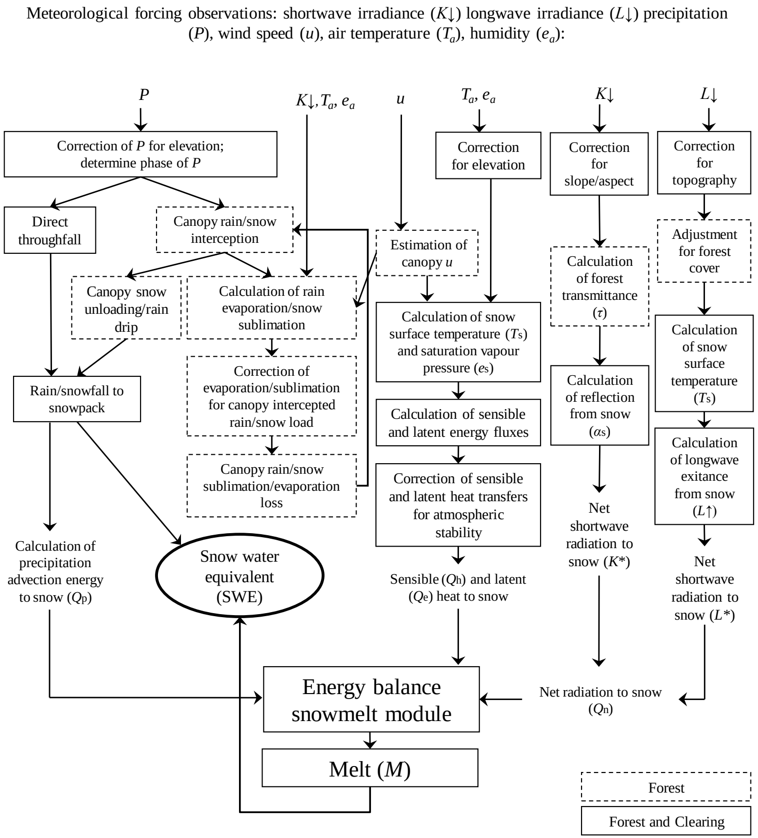

Fig. 1. Schematic outlining the major mass and energy calculations involved in the forest component of the Cold Regions Hydrological Model (CRHM).

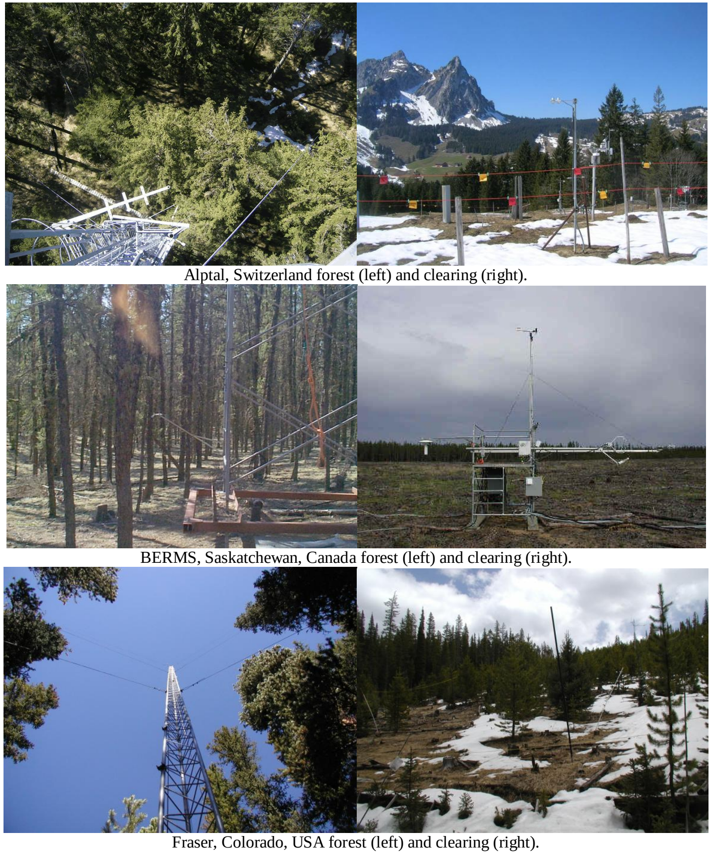

Fig. 2. Photographs of meteorological stations located at forest and clearing environments at Alptal, Switzerland; the BERMS forest site, Saskatchewan, Canada; Fraser forest, Colorado, USA and pine and spruce forests at Marmot Creek, Alberta, Canada.

HESSD

7, 1033–1072, 2010

Simulation of forest snow accumulation and melt

C. R. Ellis et al.

Marmot Creek, Alberta, Canada pine forest (left) and clearing (right).

Marmot Creek, Alberta, Canada spruce forest showing suspended spruce tree (left), clearing (centre) and radiation reference (right).

Fig. 2. Continued.

HESSD

7, 1033–1072, 2010

Title Page

Abstract | Introduction

Conclusions | References

Tables | Figures

◀| |▶

◀ ▶

Back | Close

Full Screen / Esc

Printer-friendly Version

Interactive Discussion

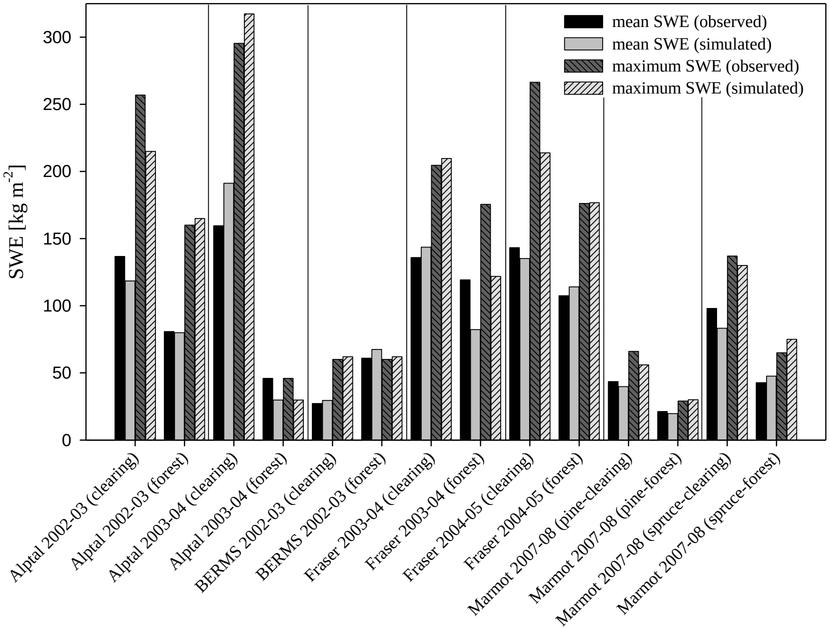

Fig. 3. Observed and simulated mean and maximum snow water equivalent (SWE) accumulations at forest and clearing sites.

HESSD

7, 1033–1072, 2010

Simulation of forest snow accumulation and melt

C. R. Ellis et al.

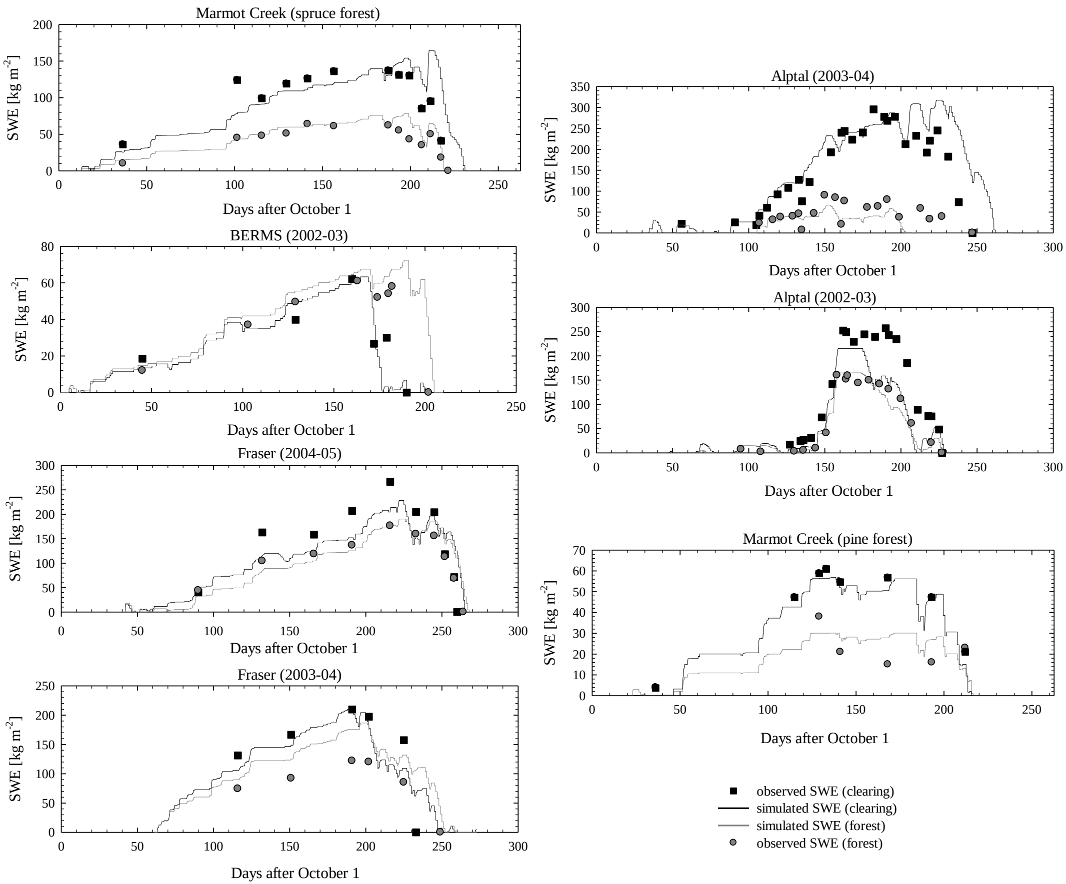

Fig. 4. Time series of observed and simulated SWE at paired clearing and forest sites.

HESSD

7, 1033–1072, 2010

Simulation of forest snow accumulation and melt

C. R. Ellis et al.

Title Page
Abstract | Introduction
Conclusions | References
Tables | Figures
◀| |▶
◀ ▶
Back | Close
Full Screen / Esc
Printer-friendly Version
Interactive Discussion

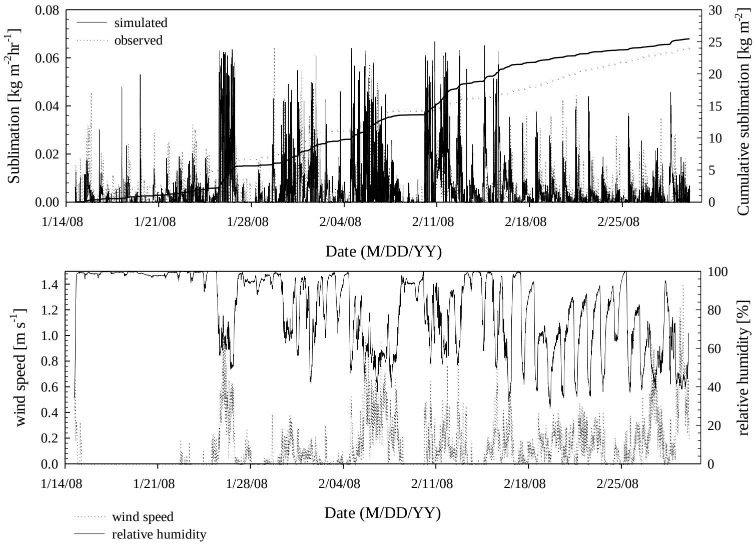

Fig. 5. Top: observed and simulated hourly (and cumulative) canopy snow sublimation; bottom: corresponding observations of forest wind speed and relative humidity.

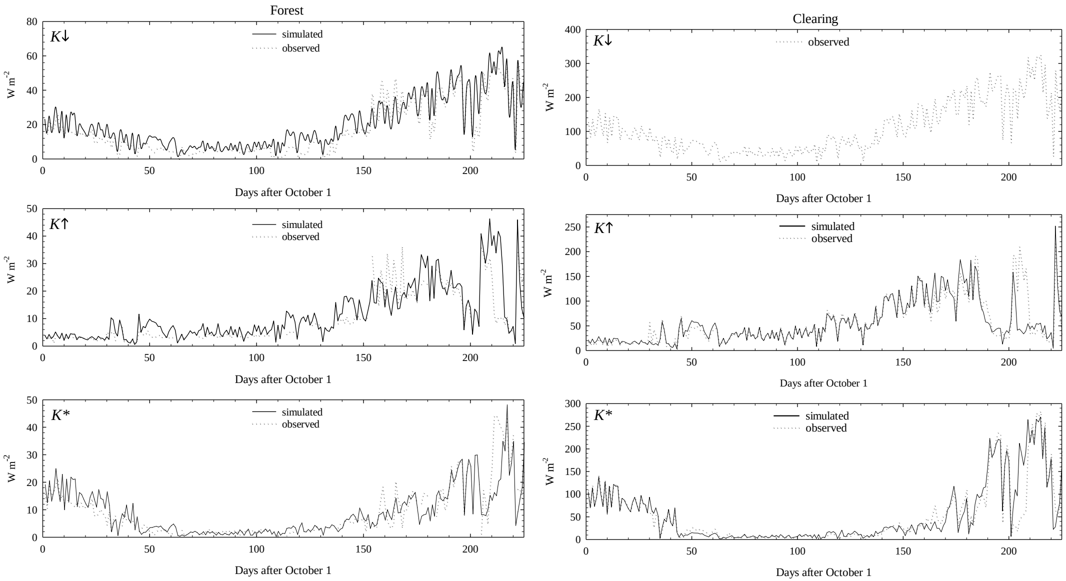

Fig. 6. Time series plots of daily average simulated and observed shortwave (K), longwave (L) radiation fluxes, and total net radiation to snow (Q_n) at pine forest and clearing sites.

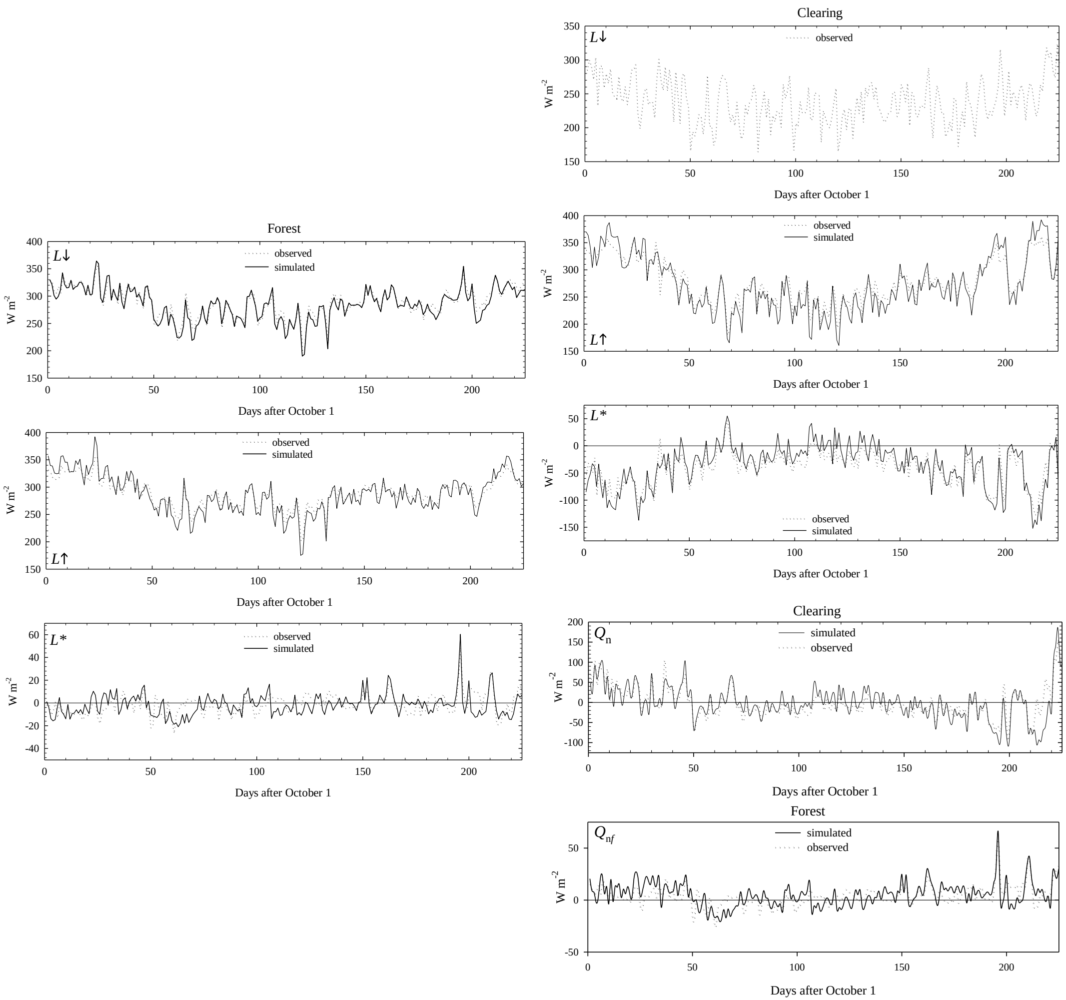

Fig. 6. Continued.

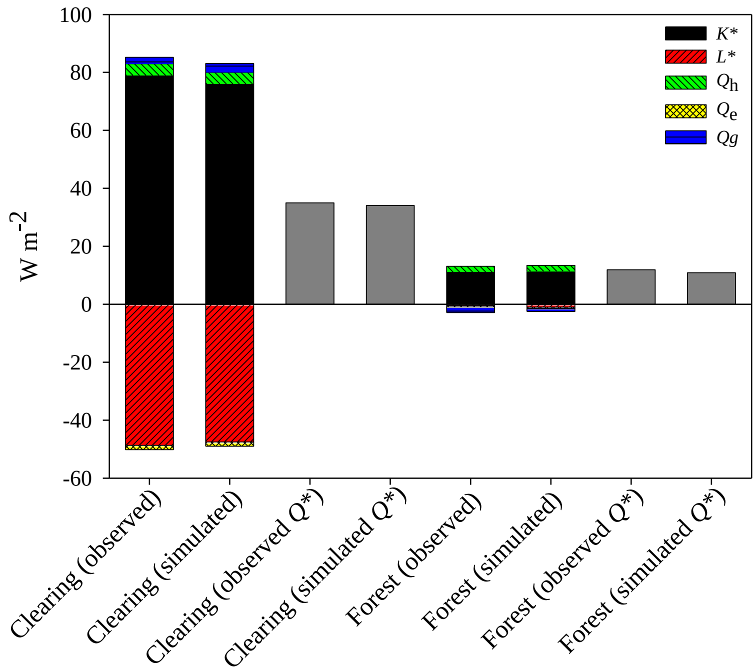

Fig. 7. Observed and simulated net energy terms and total energy to snow ($Q{*}=\mathrm{d}U/\mathrm{d}t+Q_m$) at pine forest and clearing sites (note that due to no observations of simulated sensible (Q_h) and latent (Q_e), observations are assigned the same value as simulations).